

# Nanoscale excitonic photovoltaic mechanism in ferroelectric BiFeO<sub>3</sub> thin films

Yuelin Li, Carolina Adamo, Clare E. Rowland, Richard D. Schaller, Darrell G. Schlom, and Donald A. Walko

Citation: *APL Materials* **6**, 084905 (2018); doi: 10.1063/1.5030628

View online: <https://doi.org/10.1063/1.5030628>

View Table of Contents: <http://aip.scitation.org/toc/apm/6/8>

Published by the [American Institute of Physics](#)

---

---

**PHYSICS TODAY**

WHITEPAPERS

## ADVANCED LIGHT CURE ADHESIVES

Take a closer look at what these environmentally friendly adhesive systems can do

READ NOW

PRESENTED BY  
 **MASTERBOND**  
ADHESIVES | SEALANTS | COATINGS

## Nanoscale excitonic photovoltaic mechanism in ferroelectric BiFeO<sub>3</sub> thin films

Yuelin Li,<sup>1,a</sup> Carolina Adamo,<sup>2</sup> Clare E. Rowland,<sup>3</sup> Richard D. Schaller,<sup>4</sup> Darrell G. Schlom,<sup>5,6</sup> and Donald A. Walko<sup>1</sup>

<sup>1</sup>Advanced Photon Source, Argonne National Laboratory, Argonne, Illinois 60439, USA

<sup>2</sup>Department of Applied Physics, Stanford University, Stanford, California 94305, USA

<sup>3</sup>Department of Chemistry, Northwestern University, Evanston, Illinois 60208, USA

<sup>4</sup>Center for Nanoscale Materials, Argonne National Laboratory, Argonne, Illinois 60439, USA

<sup>5</sup>Kavli Institute at Cornell for Nanoscale Science, Ithaca, New York 14853, USA

<sup>6</sup>Department of Materials Science and Engineering, Cornell University, Ithaca, New York 14853, USA

(Received 23 March 2018; accepted 23 May 2018; published online 8 June 2018)

We report an electrode-free photovoltaic experiment in epitaxial BiFeO<sub>3</sub> thin films where the picosecond optical absorption arising from carrier dynamics and piezoelectric lattice distortion due to the photovoltaic field are correlated at nanoscale. The data strongly suggest that the photovoltaic effect in phase-pure BiFeO<sub>3</sub> originates from diffusion of charge-neutral excitons and their subsequent dissociation localized at sample interfaces. This is in stark contrast to the belief that carrier separation is uniform within the sample due to the lack of center of symmetry in BiFeO<sub>3</sub>. This finding is important for formulating strategies in designing practical photovoltaic ferroelectric devices. © 2018 Author(s). All article content, except where otherwise noted, is licensed under a Creative Commons Attribution (CC BY) license (<http://creativecommons.org/licenses/by/4.0/>). <https://doi.org/10.1063/1.5030628>

Despite the significant progress in engineering optoelectronic properties of ferroelectric materials and designs for practical devices, the physical origin of the photovoltaic effect in these materials remains unclear.<sup>1</sup> Based on macroscopic and steady state measurement of photovoltage and light polarization dependence,<sup>2–4</sup> the mechanism is attributed to photo charge separation due to the lack of center of symmetry, in contrast to a conventional photovoltaic system where material or illumination inhomogeneity is necessary. The theory is termed the bulk photovoltaic effect (BPE)<sup>3</sup> with above bandgap photovoltage and an associated shift current effect.<sup>5–8</sup> Strong interfacial<sup>9,10</sup> and domain wall effects<sup>11,12</sup> also lead to a competing theory that charge separation is localized at the domain wall.<sup>11,13</sup> However, neither theory has convincing support of carrier and photo field dynamics with microscopic resolution. The material centered in the discussion is ferroelectric BiFeO<sub>3</sub>.<sup>14</sup> It exhibits strong photostriction<sup>15–18</sup> and photovoltaic effects.<sup>4,11–13,19,20</sup>

In this paper combining measurements of time-resolved spectroscopy<sup>21,22</sup> and lattice distortion,<sup>15–18</sup> we correlate the dynamics of photocarrier and the microscopic piezoelectric response in phase-pure BiFeO<sub>3</sub> thin films. The results highlight a nanoscale transient lattice distortion that is distinctly different from that expected of the BPE. The evidence strongly suggests that the photocarriers remain charge-neutral, bonded electron-hole pairs before they dissociate at the interfaces, indicating that the BPE might be a macroscopic manifestation of microscopically localized charge separations.

The experiment takes advantage of the simultaneous high temporal and spatial resolution of our methods. Briefly, we use the transient optical absorption spectroscopy (TAS) to measure optical absorption arising from the photocarrier as a function of the delay between a 40 fs, 400 nm pump laser pulse and a 1 ps, white-light probe. The absorption spectrum ranges from 400 to 750 nm. The lattice

<sup>a</sup>ylli@aps.anl.gov

distortion is measured using the time-resolved X-ray diffraction (TRXRD) technique under ambient conditions at beam line 7ID-C of the Advanced Photon Source. Optical excitation was provided by 400 nm, 50 fs laser pulses synchronized to the X-ray pulses with an adjustable time delay. Incident X-ray pulses with photon energies of 10 or 12 keV and pulse duration of 100 ps were used. The highest pump laser fluence was 5 mJ/cm<sup>2</sup>.

We employ phase-pure epitaxial (0 0 1)-oriented bismuth ferrite (BFO) thin films of 4, 20, and 35 nm grown on SrTiO<sub>3</sub> (STO) and 35 nm grown on (LaAlO<sub>3</sub>)<sub>0.3</sub>(Sr<sub>2</sub>AlTaO<sub>3</sub>)<sub>0.7</sub> (LSAT) substrates by reactive molecular-beam epitaxy.<sup>23</sup> The phase purity and high epitaxy quality of the samples were verified by the X-ray reciprocal space mapping where the 4 nm film is tetragonal and the thicker films are monoclinic.<sup>24</sup> All samples have a single domain in the sample normal direction with an in-plane domain size of 400, 40, and 40 nm for the 4, 20, and 35 nm thick samples, respectively. The pump photon energy is below the bandgaps of STO (3.2 eV) and LSAT (5 eV), thus the photo response of the substrates is negligible. For the 35-nm samples, the one grown on LSAT was used for optical measurements and the one grown on STO for the x-ray measurements. We measured no difference in the dynamics between samples with different substrates. Experimentally, piezoelectric effects are reported for BFO films below 6 nm at 8 pm/V and drop to zero at 3 nm.<sup>25</sup> Therefore, it is reasonable to assume all our samples are ferroelectric.

The generation and subsequent transport of charge carriers form an optical absorption band in a BFO following the excitation by photons with an energy larger than the direct bandgap at 2.6-2.7 eV.<sup>23</sup> The absorption spectrum spans from 1.7 to 2.5 eV, peaked at about 2.3 eV. The spectrum varies as a function of the sample thickness due to the different strain status in these films.<sup>22</sup> The relaxation of the photo-induced absorption band over time has a stretched exponential decay [Figs. 1 and 2(a)]. Defining  $\tau_{OD}$  as the 1/e relaxation time of the laser-induced optical density (OD),  $\tau_{OD}$  is found to be 0.02, 0.2, and 0.7 ns for the 4, 20, and 35 nm films, respectively.

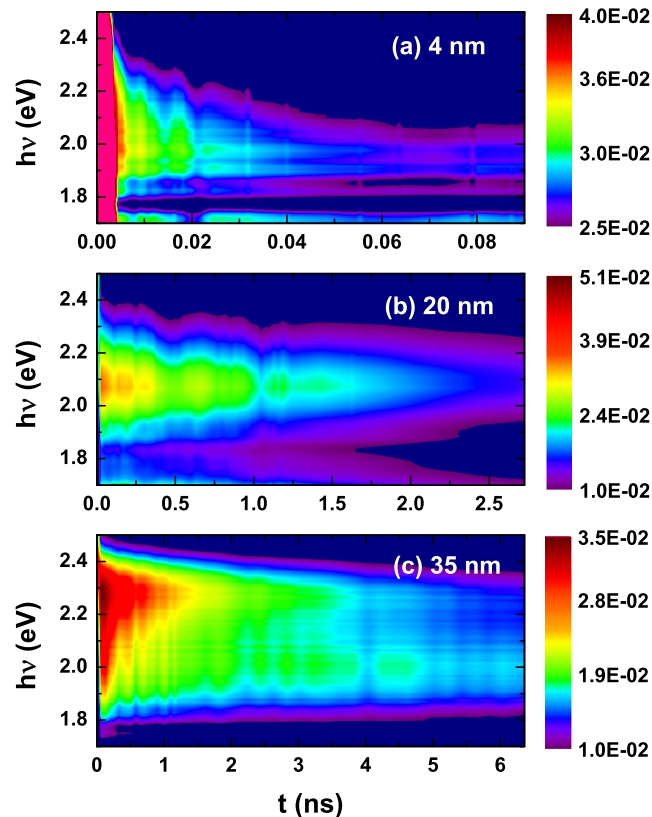


FIG. 1. TAS of the photo-induced optical density as a function of absorption photon energy and time. Note the different time scale in the (a)–(c). The nominal fluence used are 5.5, 5.5, and 4.7 mJ/cm<sup>2</sup> for the 4, 20 and 35 nm films.

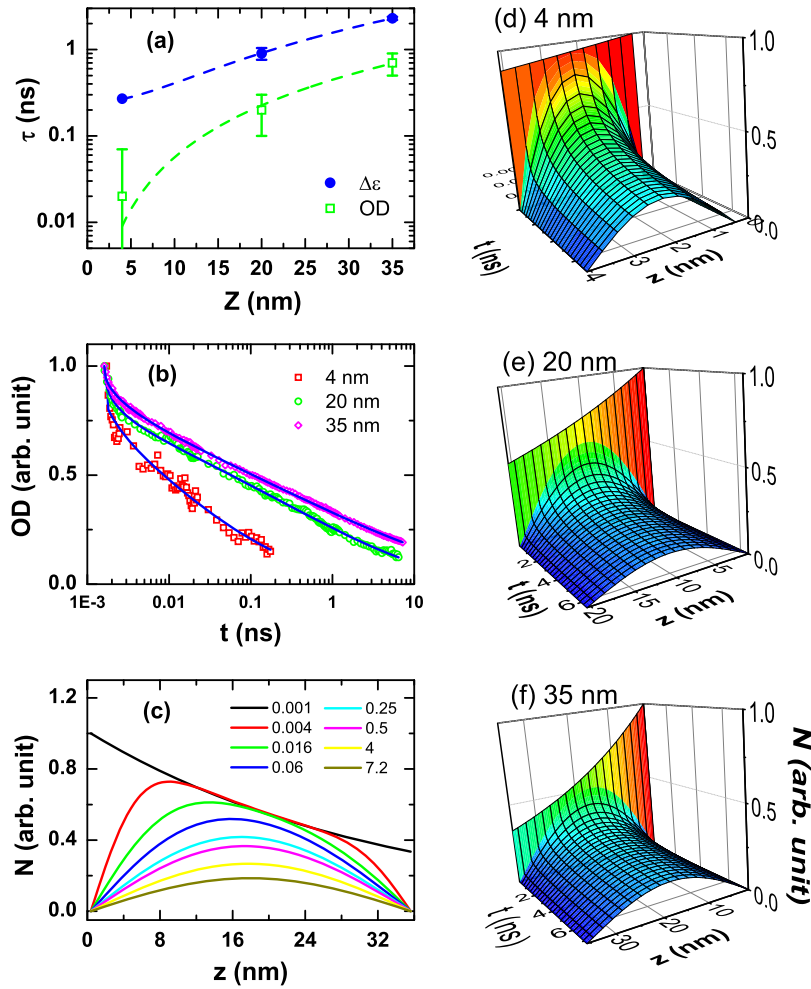


FIG. 2. (a) Recovery time for OD and average strain  $\Delta\varepsilon$  as a function of the film thickness. Note that the samples have a linear response to the pump laser fluence, i.e., the peak OD and strain are linearly dependent on the laser fluence with constant relaxation time for each sample thickness. The measured recovery time in (a) is the average over measurements at three pump fluences, with error bars representing the standard deviation. The dashed curves are fits to a second-order polynomial function, with the second-order terms dominating the OD signal. (b) Fitting of the OD as a function of time by solving the diffusion equations (1)–(3) using the cases in Fig. 1. (c) The carrier density profile at selected times (given in ns) from the best fit for the 35 nm film. [(d)–(f)] Carrier dynamics as a function of time and film depth. The fitting parameters are  $\gamma = 0.79, 0.82,$  and  $0.82$  and  $D = 1.7, 16,$  and  $55 \text{ nm}^2/\text{ps}^{1-\gamma}$  for the 4, 20, and 35 nm films, respectively.

The decay of the absorption is due to carrier removal from the system through recombination or dissociation. The lifetime of the carrier can be expressed as  $1/\tau_{OD} = 1/\tau_B + 1/\tau_S$ , where  $\tau_B$  and  $\tau_S$  are due to the recombination/dissociation in the bulk and at the sample surfaces,<sup>26</sup> where we have  $\tau_S = Z/s + (Z/\pi)^2/D$ , with  $Z$  as the sample thickness,  $s$  as the surface quenching velocity, and  $D$  as the diffusion coefficient, respectively. Clearly, a strong thickness dependence indicates that  $\tau_B \gg \tau_S$  and within our resolution,  $\tau_{OD} = \tau_S$ , i.e., carrier quenching is dominated by surface/interface effects. Further analysis shows that  $\tau_{OD}$  is quadratically dependent on the film thickness [see Fig. 2(a)], indicating quenching is much faster than diffusion in these samples. Thus, the carrier dynamics is dominated by their diffusion. This largely rules out the possibility that the carriers are locally trapped entities as previously speculated.<sup>22</sup>

Stretched exponential decay is associated with a diffusion system with traps (in our case, self-trapping), which can be described by a diffusion model using a time-dependent diffusion constant.<sup>27</sup> The one-dimensional diffusion equation, widely applied in describing the carrier dynamics in excitonic photovoltaic devices,<sup>28</sup> can be written as

$$\frac{\partial}{\partial t} N(t, z) = \frac{\partial}{\partial z} \left( D t^{-\gamma} \frac{\partial}{\partial z} N(t, z) \right). \quad (1)$$

Here  $N$  is the carrier density, and  $D(t) = D t^{-\gamma}$  is the diffusion coefficient with  $1 > \gamma > 0$ , where  $\gamma$  is a measure of the trap energy distribution.<sup>27</sup> The initial and boundary conditions are

$$N(0, z) \propto \exp\left(-\frac{z}{L}\right), \quad (2)$$

$$\frac{\partial}{\partial z} N(t, z) / N(t, z) = \frac{s(z)}{D(t)} \Big|_{z=0 \text{ or } Z} \gg 1. \quad (3)$$

In these equations,  $L$  is the optical absorption length,<sup>14</sup>  $z = 0$  is the interface between the film and air,  $z = Z$  is at the film/substrate interface, and  $s$  is the surface quenching velocity. The equation can be solved by adjusting  $D$  and  $\gamma$  while fitting to the measured OD time dependence so that  $OD(t) \propto \int N(z, t) dz$ . As shown in Fig. 2(b), the observed OD dynamics is closely reproduced by the fitting. The spatiotemporal carrier diffusion maps are shown in Figs. 2(c)–2(f).

Correlated to the TAS results, a thickness dependence of the film structural distortion was also observed in the TRXRD measurement, shown in Fig. 2(a) for the shift of the (0 0 2) BFO diffraction peak, or the average strain. Note that the strain has a longer relaxation time because heating also contributes to the expansion of the lattice with a much longer time scale.<sup>16</sup> The diffraction peak after the laser excitation shifts to lower diffraction angle indicating the expansion of the lattice [Fig. 3(a)]. The thickness dependence is consistent with the TAS data. As discussed earlier, it also rules out any localized, non-diffusive effect as the dominant origin of the lattice distortion as previously speculated.<sup>18,29</sup>

To reveal the structure distortion mechanism, we performed a measurement of the time-dependent strain profile, i.e., the depth-dependent lattice distortion. This is accomplished by measuring the diffraction intensity distribution along a large range of reciprocal space [Fig. 3(a)], which is the convolution of the phase distribution of the reflected X-ray along the film depth due to the distortion of the individual unit cell layer.<sup>30,31</sup> The strain profile is first retrieved using the Gerchberg–Saxton algorithm, followed by a six-point spline algorithm fitting the phase and the layer-by-layer occupancy of the BFO unit cell.<sup>30,31</sup> The fitting to the data, as shown in Fig. 3(b) for the 35 nm film, provides an excellent agreement to the measured diffraction intensity distribution and a detailed strain profile, a significant improvement over the results published previously.<sup>17</sup> It shows that the depth-dependent strain profile as a function of time after the photoexcitation [Fig. 3(c)] is linearly dependent on the strain profile before the photo excitation

$$\varepsilon(t, z) = \alpha(t)\varepsilon_0(z) + \beta(t). \quad (4)$$

Here  $\varepsilon_0(z)$  is the strain profile before the laser excitation. Both  $\beta(t)$  and  $\alpha(t)$  are correlated to the shift of the diffraction peak.

After excluding other candidate effects,<sup>17</sup> the time-dependent strain profile is consistent with a piezoelectric response of the film to a spatially homogeneous but time-dependent electric field across the film depth, i.e., the screening field. This can be shown by rewriting Eq. (4) as follows:

$$\varepsilon(t, z) = E(t)d_{33}(z) + \varepsilon_{th}(t), \quad (5)$$

where  $d_{33}(z) \propto \varepsilon_0(z)$  is the piezoelectric coefficient,  $\varepsilon_{th}(t) \propto \beta(t)$  is a homogeneous strain over the sample that can be attributed to heating,<sup>16</sup> and  $E(t) \propto \alpha(t)$  is a spatially homogeneous screening field due to free carriers accumulated (destroyed) at the interfaces from the dissociated laser generated excitons. Note that though  $d_{33}$  is commonly used as a constant, it is both a function of the external electric field in lead zirconate titanate (PZT)<sup>32,33</sup> and the strain in the BFO, as analyzed before.<sup>17,34</sup>

The spatial uniformity of the screening field  $E(t)$  across the film implies that the film behaves like a planar capacitor, indicating that there is no significant presence of free carriers in the bulk of the film, i.e., photocarriers remain charge neutral entities before their arrival at the interfaces. These carriers dissociate at the interfaces, and electron and holes are separated by the polarization field to

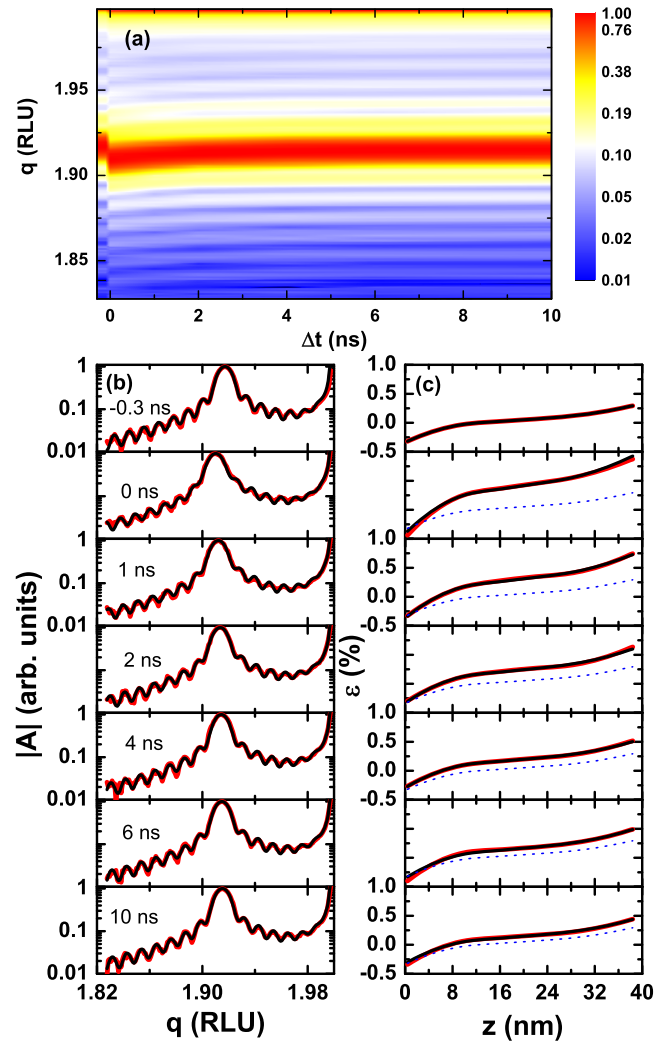


FIG. 3. (a) Diffraction intensity as a function of delay along the truncation rod around the (0 0 2) diffraction peak for a 35 nm BFO thin film, interpolated from measurement at time  $\Delta t = -0.3, 0, 1, 2, 4, 6,$  and  $10$  ns. (b) Measured (red thick lines) and fitted (black thin lines) diffraction amplitude  $|A|$  at different delays. (c) Corresponding retrieved (red thick lines) and fitted (black thin lines) strain profiles using Eq. (4) at different delays, in comparison with that before the optic excitation (dotted line). The lower strain side is determined to be the air/film interface based on the relaxation of epitaxial strain. The fitting overlaps with the data within the thickness of the line in (b) and (c). RLU: reciprocal lattice unit referencing to the STO substrate. Note that we added 4 monolayers ( $\sim 1.6$  nm) at the air/substrate interfaces to accommodate the roughness (partial occupancy), where the retrieved strain may contain larger uncertainties.

form the screening field, a completely different scenario from the BPE. To confirm this, we simulate the piezoelectric response of the film due to BPE using a self-consistent one-dimensional particle-in-cell model<sup>35</sup> for the 35 nm film. Equal number of holes and electrons is generated, filling the space following the laser deposition profile  $p(z) \propto \exp(-z/L)$ . To simulate the internal polarization field, a hypothetical constant bias field  $E_0 = 1$  MV/cm (screened by the surface charges, the remaining field can be much smaller) is applied to generate a peak strain of 0.5% that is comparable to the data (for a  $d_{33} = 50$  pm/V with a dielectric constant of 50<sup>14</sup>). We use nominal mobility for the electrons and holes of  $7 \times 10^{-5}$  and  $5 \times 10^{-5}$   $\text{m}^2 \text{V}^{-1} \text{s}^{-1}$ , respectively. The carriers are absorbed when they reach the boundaries. Figure 4 is a case with a carrier density of  $1.5 \times 10^{18}$   $\text{cm}^{-3}$  (absorption fluence of 0.005  $\text{mJ}/\text{cm}^2$ ) where the bulk charge separation causes  $\pm 50\%$  modulation of the field inside the film. The resulting strain profile, and thus the diffraction intensity distribution, is however completely different from the experimental observation [Figs. 4(b) and 4(c)], eliminating the role of the BPE

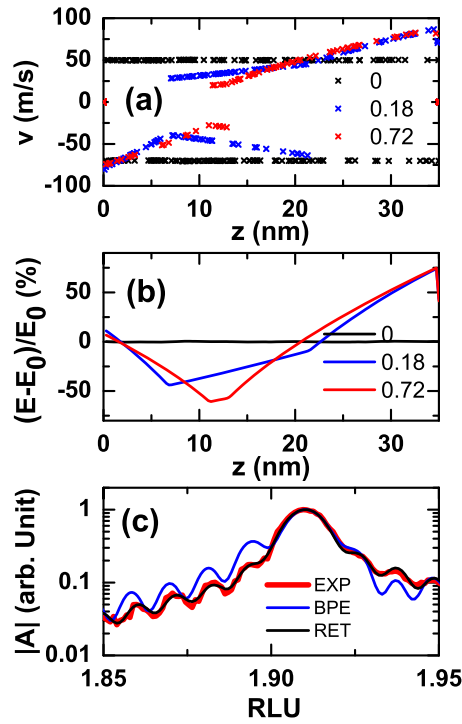


FIG. 4. Comparison of strain effects in a 35 nm film due to BPE with experiment data. (a) Position-velocity diagram of the holes (positive speed) and electrons (negative speed) at different times (indicated in the legend in nanoseconds) after the impulsive excitation; (b) the corresponding fields due to charge separation by the internal field of  $E_0 = 1$  MV/cm; and (c) simulated (0 0 2) diffraction pattern (blue) due to the lattice response to the field in (b) in comparison with the experiment (red line) and the retrieval (black thin line) data.

mechanism in our experiment. Note that this model is not intended to describe the BFO material. The case for Dember field<sup>36</sup> is not applicable because the polarization field would drive electrons and holes, if present in the bulk, to opposite directions.

The difference of nanoscale piezoelectric response between the bulk and interface charge separation effects is transient and thus can only be revealed via a time-resolved measurement with nanoscale spatial resolution. The difference disappears once a steady current is established, and electrons and holes mix homogeneously in the film.

One plausible structure of the charge-neutral carrier can be inferred from the spectral feature at 1.8–2.4 eV in Fig. 1. This spectral structure has been identified as the electronic origin of the photostriction effect in the thin film BFO<sup>16</sup> and more recently the origin of photovoltaic effect in BFO single crystals.<sup>37</sup> It has been interpreted as a characteristic of a self-trapped charge transfer (CT) exciton with a hole in the O-2p orbitals and an extra electron in the Fe-3d orbitals.<sup>38</sup> Such a self-trapped CT exciton in oxides has been discussed as an inherent material property<sup>38,39</sup> of which the hopping is facilitated by the lattice distortion. The dissociation of the exciton at the interfaces can be due to local band bending,<sup>40</sup> band line up,<sup>41</sup> defects,<sup>42</sup> or pre-existing free carriers. Such localized exciton dissociation is consistent with the well-documented domain wall and interface effects,<sup>9–12</sup> but the details remain to be understood. Note that due to the charge neutrality of CT excitons, the diffusion dynamics is not dependent on the sample polarization. The piezo effect due to the screening of the depolarization field by dissociated carrier always enhances the polarization field and is not dependent on the poling of the film either. Some of the surface quenching processes may be dependent on the polarization, but our present technique is not capable of resolving such dependence.

For bulk samples, the exciton mechanism is not directly observable due to the limited exciton diffusion length. However, even in a macroscopic sample, excitons need not traverse the whole sample to generate free carriers—they only need to diffuse far enough to reach entities such as grain

boundaries, defects, or electrodes to generate free carriers which in turn can be separated by the internal polarization field. This would lead to the appearance as if the bulk contributed to the photovoltaic effect homogeneously. Physical pictures of a bulk effect based on such micro/nano processes have been proposed before<sup>1,11,13,43</sup> but lack the evidence of corresponding carrier and photovoltaic field dynamics. The role of the interplay between the excitons and the light field in generating the shift current remains to be understood.

Note that our samples have no electrodes, preventing us from performing some of the standard photovoltaic measurements. However, it is worth mentioning that the strain dynamics in our experiments serve as a location-sensitive nanoscale field sensor. This allows the corroboration of the field distribution with the carrier dynamics on a picosecond time scale with nanometer resolution, which cannot be achieved in a conventional photovoltaic measurement of the photovoltage or current. The nanoscale excitonic mechanism opens a new perspective for understanding the photovoltaic effect in ferroelectric materials and may lead to very different design strategies for practical devices.

Work at Argonne was supported by the U.S. Department of Energy, Office of Science, Office of Basic Energy Sciences, under Contract No. DE-AC02-06CH11357, and by the American Recovery and Reinvestment Act (ARRA) funding through the Office of Advanced Scientific Computing Research under Contract No. DE-AC02-06CH11357. Work at Cornell University was supported by the Army Research Office through Agreement No. W911NF-08-2-0032.

- <sup>1</sup> K. T. Butler, J. M. Frost, and A. Walsh, *Energy Environ. Sci.* **8**, 838 (2015).
- <sup>2</sup> A. M. Glass, *Appl. Phys. Lett.* **25**, 233 (1974).
- <sup>3</sup> V. M. Fridkin, *Crystallogr. Rep.* **46**, 654 (2001).
- <sup>4</sup> T. Choi, S. Lee, Y. J. Choi, V. Kiryukhin, and S.-W. Cheong, *Science* **324**, 63 (2009).
- <sup>5</sup> S. M. Young, F. Zheng, and A. M. Rappe, *Phys. Rev. Lett.* **109**, 236601 (2012).
- <sup>6</sup> D. Daranciang, M. Highland, H. Wen, S. Young, N. Brandt, H. Hwang, M. Vattilana, M. Nicoul, F. Quirin, J. Goodfellow, T. Qi, I. Grinberg, D. Fritz, M. Cammarata, D. Zhu, H. Lemke, D. Walko, E. Dufresne, Y. Li, J. Larsson, D. Reis, K. Sokolowski-Tinten, K. Nelson, A. Rappe, P. Fuoss, G. Stephenson, and A. Lindenberg, *Phys. Rev. Lett.* **108**, 087601 (2012).
- <sup>7</sup> A. M. Cook, B. M. Fregoso, F. de Juan, S. Coh, and J. E. Moore, *Nat. Commun.* **8**, 14176 (2017).
- <sup>8</sup> Z. Gu, D. Imbrenda, A. L. Bennett-Jackson, M. Falmbigl, A. Podpirka, T. C. Parker, D. Shreiber, M. P. Ivill, V. M. Fridkin, and J. E. Spanier, *Phys. Rev. Lett.* **118**, 096601 (2017).
- <sup>9</sup> F. Zheng, J. Xu, L. Fang, M. Shen, and X. Wu, *Appl. Phys. Lett.* **93**, 172101 (2008).
- <sup>10</sup> G.-L. Yuan and J. Wang, *Appl. Phys. Lett.* **95**, 252904 (2009).
- <sup>11</sup> S. Y. Yang, J. Seidel, S. J. Byrnes, P. Shafer, C.-H. Yang, M. D. Rossell, P. Yu, Y.-H. Chu, J. F. Scott, J. W. Ager, L. W. Martin, and R. Ramesh, *Nat. Nanotechnol.* **5**, 143 (2010).
- <sup>12</sup> M.-M. Yang, A. Bhatnagar, Z.-D. Luo, and M. Alexe, *Sci. Rep.* **7**, 43070 (2017).
- <sup>13</sup> J. Seidel, D. Fu, S.-Y. Yang, E. Alarcón-Lladó, J. Wu, R. Ramesh, and J. W. Ager, *Phys. Rev. Lett.* **107**, 126805 (2011).
- <sup>14</sup> G. Catalan and J. F. Scott, *Adv. Mater.* **21**, 2463 (2009).
- <sup>15</sup> B. Kundys, M. Viret, D. Colson, and D. O. Kundys, *Nat. Mater.* **9**, 803 (2010).
- <sup>16</sup> H. Wen, P. Chen, M. Cosgriff, D. Walko, J. Lee, C. Adamo, R. Schaller, J. Ihlefeld, E. Dufresne, D. Schlom, P. Evans, J. Freeland, and Y. Li, *Phys. Rev. Lett.* **110**, 037601 (2013).
- <sup>17</sup> Y. Li, C. Adamo, P. Chen, P. G. Evans, S. M. Nakhmanson, W. Parker, C. E. Rowland, R. D. Schaller, D. G. Schlom, D. A. Walko, H. Wen, and Q. Zhang, *Sci. Rep.* **5**, 16650 (2015).
- <sup>18</sup> C. Paillard, B. Xu, B. Dkhil, G. Geneste, and L. Bellaïche, *Phys. Rev. Lett.* **116**, 247401 (2016).
- <sup>19</sup> W. Ji, K. Yao, and Y. C. Liang, *Adv. Mater.* **22**, 1763 (2010).
- <sup>20</sup> Y.-T. Peng, S.-H. Chiou, C.-H. Hsiao, C. (Hao) Ouyang, and C.-S. Tu, *Sci. Rep.* **7**, 45164 (2017).
- <sup>21</sup> Y. M. Sheu, S. A. Trugman, Y.-S. Park, S. Lee, H. T. Yi, S.-W. Cheong, Q. X. Jia, A. J. Taylor, and R. P. Prasankumar, *Appl. Phys. Lett.* **100**, 242904 (2012).
- <sup>22</sup> Y. Yamada, T. Nakamura, S. Yasui, H. Funakubo, and Y. Kanemitsu, *Phys. Rev. B* **89**, 035133 (2014).
- <sup>23</sup> J. F. Ihlefeld, N. J. Podraza, Z. K. Liu, R. C. Rai, X. Xu, T. Heeg, Y. B. Chen, J. Li, R. W. Collins, J. L. Musfeldt, X. Q. Pan, J. Schubert, R. Ramesh, and D. G. Schlom, *Appl. Phys. Lett.* **92**, 142908 (2008).
- <sup>24</sup> Y. Yang, C. M. Schlepütz, C. Adamo, D. G. Schlom, and R. Clarke, *APL Mater.* **1**, 052102 (2013).
- <sup>25</sup> J. L. Zhao, H. X. Lu, J. R. Sun, and B. G. Shen, *Phys. B* **407**, 2258 (2012).
- <sup>26</sup> A. B. Sproul, *J. Appl. Phys.* **76**, 2851 (1994).
- <sup>27</sup> J. Kakalios, R. A. Street, and W. B. Jackson, *Phys. Rev. Lett.* **59**, 1037 (1987).
- <sup>28</sup> G. Xing, N. Mathews, S. Sun, S. S. Lim, Y. M. Lam, M. Gratzel, S. Mhaisalkar, and T. C. Sum, *Science* **342**, 344 (2013).
- <sup>29</sup> D. Schick, M. Herzog, H. Wen, P. Chen, C. Adamo, P. Gaal, D. G. Schlom, P. G. Evans, Y. Li, and M. Bargheer, *Phys. Rev. Lett.* **112**, 097602 (2014).
- <sup>30</sup> I. Vartanyants, C. Ern, W. Donner, H. Dosch, and W. Caliebe, *Appl. Phys. Lett.* **77**, 3929 (2000).
- <sup>31</sup> A. Boulle, O. Masson, R. Guinebrière, and A. Daurer, *J. Appl. Crystallogr.* **36**, 1424 (2003).
- <sup>32</sup> V. Nagarajan, A. Stanishevsky, L. Chen, T. Zhao, B.-T. Liu, J. Melngailis, A. L. Roytburd, R. Ramesh, J. Finder, Z. Yu, R. Droopad, and K. Eisenbeiser, *Appl. Phys. Lett.* **81**, 4215 (2002).
- <sup>33</sup> Z. Zhao, Z. Luo, C. Liu, W. Wu, C. Gao, and Y. Lu, *Rev. Sci. Instrum.* **79**, 064704 (2008).

- <sup>34</sup> C. Daumont, W. Ren, I. C. Infante, S. Lisenkov, J. Allibe, C. Carrétéro, S. Fusil, E. Jacquet, T. Bouvet, F. Bouamrane, S. Prosandeev, G. Geneste, B. Dkhil, L. Bellaiche, A. Barthélémy, and M. Bibes, *J. Phys.: Condens. Matter* **24**, 162202 (2012).
- <sup>35</sup> J. M. Dawson, *Rev. Mod. Phys.* **55**, 403 (1983).
- <sup>36</sup> T. Dekorsy, H. Auer, H. J. Bakker, H. G. Roskos, and H. Kurz, *Phys. Rev. B* **53**, 4005 (1996).
- <sup>37</sup> M. Yang, A. Bhatnagar, and M. Alexe, *Adv. Electron. Mater.* **1**, 1500139 (2015).
- <sup>38</sup> R. Pisarev, A. Moskvina, A. Kalashnikova, and T. Rasing, *Phys. Rev. B* **79**, 235128 (2009).
- <sup>39</sup> V. Vikhnin, R. Eglitis, S. Kapphan, G. Borstel, and E. Kotomin, *Phys. Rev. B* **65**, 104304 (2002).
- <sup>40</sup> L. Pintilie and M. Alexe, *J. Appl. Phys.* **98**, 124103 (2005).
- <sup>41</sup> R. Schafranek, J. D. Baniecki, M. Ishii, Y. Kotaka, and K. Kurihara, *New J. Phys.* **15**, 053014 (2013).
- <sup>42</sup> T. Rojac, A. Bencan, G. Drazic, N. Sakamoto, H. Ursic, B. Jancar, G. Tavcar, M. Makarovic, J. Walker, B. Malic, and D. Damjanovic, *Nat. Mater.* **16**, 322 (2016).
- <sup>43</sup> P. S. Brody and F. Crowne, *J. Electron. Mater.* **4**, 955 (1975).